COMPUTER VISION-BASED IMAGE ANALYSIS TO CHARACTERIZE TURBULENT STRONGLY COUPLED DUSTY PLASMA

V. Gaciu[1,2], D. Ticoș[3], N. Udrea[3], M.L. Mitu[3], A. Scurtu[3], C.M. Ticoș[1,2,3]

Strongly coupled dusty plasmas can exhibit turbulent behavior when externally driven by a collimated electron beam with energies in the keV range. The energetic electrons exert a drag force on the negatively charged dust particles, inducing a flow with typical velocities on the order of several millimeters per second. Simultaneously, Coulomb repulsion between particles influences their dynamics, often resulting in irregular and erratic trajectories. The resulting dust flow is captured using a high-speed camera, and Particle Image Velocimetry (PIV) is employed to extract the velocity field. From this, the vorticity distribution is computed to characterize the local rotational features of the flow. In this study, we apply video processing techniques—including contour detection, color-based segmentation, and Principal Component Analysis (PCA)—to analyze turbulent regions within the vorticity maps. These methods enable both qualitative visualization and quantitative assessment of flow structures. The entire implementation is carried out in Python using the OpenCV library.

Keywords Image processing, computer vision, laser illumination, electron beam, plasma crystal, turbulence, PCA.

1. Introduction

Strongly coupled dusty plasmas are unique states of matter where charged dust particles, typically micrometer-sized, are suspended in a plasma environment and interact intensely with each other due to their high electric charges [1]. Unlike conventional plasmas, where ions and electrons dominate, the presence of massive dust grains introduces unique dynamics, leading to strong Coulomb coupling that can result in liquid-like or even crystalline behaviors, such as the formation of plasma crystals [2, 3, 4, 5, 6]. These systems bridge

[1]Engineering and Applications of Lasers and Accelerators Doctoral School (SDIALA), National University of Science and Technology Politehnica of Bucharest, 313 Splaiul Independenţei St., Bucharest RO-060042, Romania, e-mail:b vlad.gaciu@eli-np.ro

[2] Extreme Light Infrastructure-Nuclear Physics (ELI-NP), Horia Hulubei National Institute for R&D in Physics and Nuclear Engineering, Magurele 077125, Romania

[3] National Institute for Laser, Plasma and Radiation Physics, Atomistilor Street 409, Magurele, Ilfov 077125, Romania

plasma physics, condensed matter, and soft matter, offering insights into fundamental processes like self-organization, phase transitions, and wave phenomena. Found in astrophysical settings like planetary rings and comet tails, as well as in laboratory and industrial applications such as semiconductor processing, strongly coupled dusty plasmas are a rich field for studying complex, non-equilibrium systems [7, 8].

Plasma crystals, formed in strongly coupled dusty plasmas, exhibit remarkable responses when subjected to external forces, such as those induced by the pressure of a laser beam or an electron beam [9]. These forces can manipulate the charged dust particles arranged in ordered, crystalline structures, driving dynamic behaviors like controlled oscillations, lattice deformations, or even directed particle flows. For instance, laser beams exert radiation pressure that can shear or compress the crystal, triggering phase transitions or wave propagation, while electron beams introduce localized perturbations by altering the charge and interaction potential of the dust grains [10, 11, 12, 13, 14, 15, 16, 17]. Such external driving forces enable control and tuning over the plasma crystal's structure and dynamics, making them valuable for studying non-equilibrium phenomena and collective excitations [18].

Recent studies have demonstrated that a collimated electron beam, with an energy of approximately 13 keV, exerts a significant drag force on dust particles within a strongly coupled dusty plasma, inducing a directed flow with velocities reaching several millimeters per second [19, 20, 21]. This external force, combined with the intrinsic Coulomb coupling between highly charged dust grains, results in complex particle dynamics, where the particles exhibit chaotic trajectories superimposed on the overall drift [19]. Within a quasi-2-dimensional plasma crystal, this interplay leads to a turbulent state characterized by the formation of local vortices of varying sizes and vorticity. These vortices continuously emerge and dissipate within the flow, driving non-equilibrium dynamics.

The presence of vortices alone does not guarantee a turbulent flow, particularly in the context of shear layers formed between rapidly moving dust particles, driven by the drag force of the electron beam, and stationary dust particles locked in a crystalline lattice [22, 23, 24, 25, 26]. However, the observed velocity fluctuations and the chaotic trajectories of the particles strongly suggest that the flow exhibits turbulent characteristics [9].

Vorticity characterizes the local rotational motion of dust flow and plays a central role in the dynamics of turbulent flows. To be able to quantify the turbulent flow, an important metric is the statistical characterization of vortices, including their number and size, typically represented by their area or volume. Additionally, the directional distribution of vorticity within vortices can provide valuable insights into the local flow structure and may be essential for a complete understanding of energy transfer mechanisms within the turbulent regime [27].

2. Experimental setup

To analyze the flow dynamics, high-speed video imaging captures the motion of dust particles from a top-down perspective as shown in Fig. 1. Particle image velocimetry (PIV) is then used to map the local flow vectors [28]. From these, the local vorticity is calculated, revealing the turbulent structure of the flow, as illustrated in the accompanying vorticity map shown in Figure 2.

A dust flow is generated by irradiating a stable quasi-2-dimensional plasma crystal with an electron beam at an energy of 13 keV and a beam current of 4 mA. The plasma crystal consists of identical plastic spheres, each with a diameter of 11.8 μm and is levitated in the sheath region of a radio-frequency (RF) argon plasma discharge at a pressure of 84 mTorr. The dust particles become electrically charged through interactions with the electron and ion fluxes from the plasma, acquiring a steady negative charge of approximately 14.9×10^3 elementary charges $e = -1.6 \times 10^{-19}$ C. They are typically levitated near the bottom RF electrode, within the sheath region that separates the plasma from the electrode. In this region, the sheath electric field exerts an upward electric force on the negatively charged particles, balancing the downward gravitational force.

The crystal is illuminated by a laser sheet generated by passing the beam of a continuous-wave (CW) laser diode with an optical power of 20 mW through a cylindrical lens. This configuration illuminates only the region where the dust particle structure is located, providing sufficient intensity to make the particles visible through laser light scattering.

The electron beam is monoenergetic and produced by accelerating electrons emitted from a pulsed hollow-anode Penning discharge using a round, hollow extractor electrode biased at a fixed high voltage of 13 kV. After acceleration, the electron bunch passes through two successive coaxial coils that generate adjustable axial magnetic fields in the range of 10 to 200 G. Finally, the beam is directed through a small orifice with a diameter of 0.5 mm and aimed at the levitated dust crystal inside the experimental chamber. The beam has a divergence of approximately 3.2°, resulting in a spot size of about 5 mm in diameter at the interaction region with the dust crystal.

A high-speed CMOS camera (Photron FASTCAM UX100) equipped with a Micro-Nikkor lens of 55 mm focal length and an additional $\times 2$ magnifying lens is operated at approximately 125 frames per second to record up to 1000 images of the dust flow dynamics, corresponding to a continuous recording duration of about 8 seconds. The camera is typically activated just before the onset of the electron beam, but only the sequence recorded after the first 500 milliseconds is considered for analysis in order to exclude transient effects occurring at the beginning of the interaction. The acquired image sequence is processed using a time-resolved (PIV) software (by LaVision) to compute local dust flow velocity vectors from consecutive frames. More details of the

experimental setup, depicted in Figure 1, are available in the referenced work [9]. The vorticity shown in Figure 2 is calculated from the PIV velocity vectors in both directions, v_x and v_y, using the relation $\omega = \partial v_y/\partial x - \partial v_x/\partial y$.

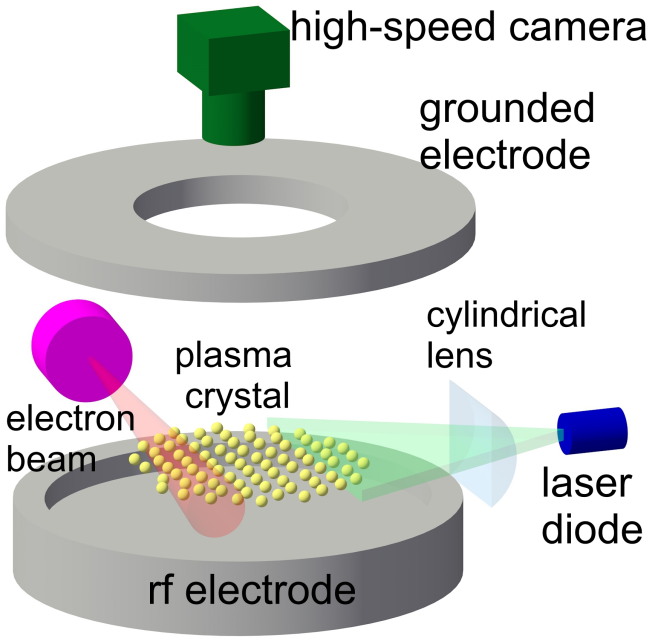

FIGURE 1. Experimental setup for obtaining an electron beam induced dust flow in a quasi-2-dimensional plasma crystal levitated above the RF electrodes.

Image processing plays a crucial role even in plasma physics, particularly when imaging sensors are involved, as is common in fields like computer vision, medical imaging, and autonomous systems. A fundamental approach to achieving object boundaries within points of the same color or intensity is color segmentation for contour detection. Contours are useful in object detection, object recognition, and shape analysis [29]. Typically, contour detection is achieved by first applying an edge-detection algorithm. In our case, with color being a distinguishing feature, color segmentation is the best approach. Color segmentation is used to isolate the hues of red and blue that we are attempting to find and contour. This paper focuses on generating contours for red and blue regions in the image, and applying principal component analysis (PCA) vectors to visualize the direction of the underlying pattern inside individual vortices.

3. Methodology

Our image begins as a 2D function $I(x, y)$, in which we want to find contours of only red and blue regions. Here, I represents the intensity pixel

values along the x and y directions. $I(x, y)$ does not represent a physical quantity but rather a numerical measure of image brightness. We perform edge detection by taking the gradient ∇I, and marking edges as the points with high changes of intensity. Contours can be defined as $I(x, y) = c$, and tracing the contours is done using the topological traversal of edge-connected pixels.

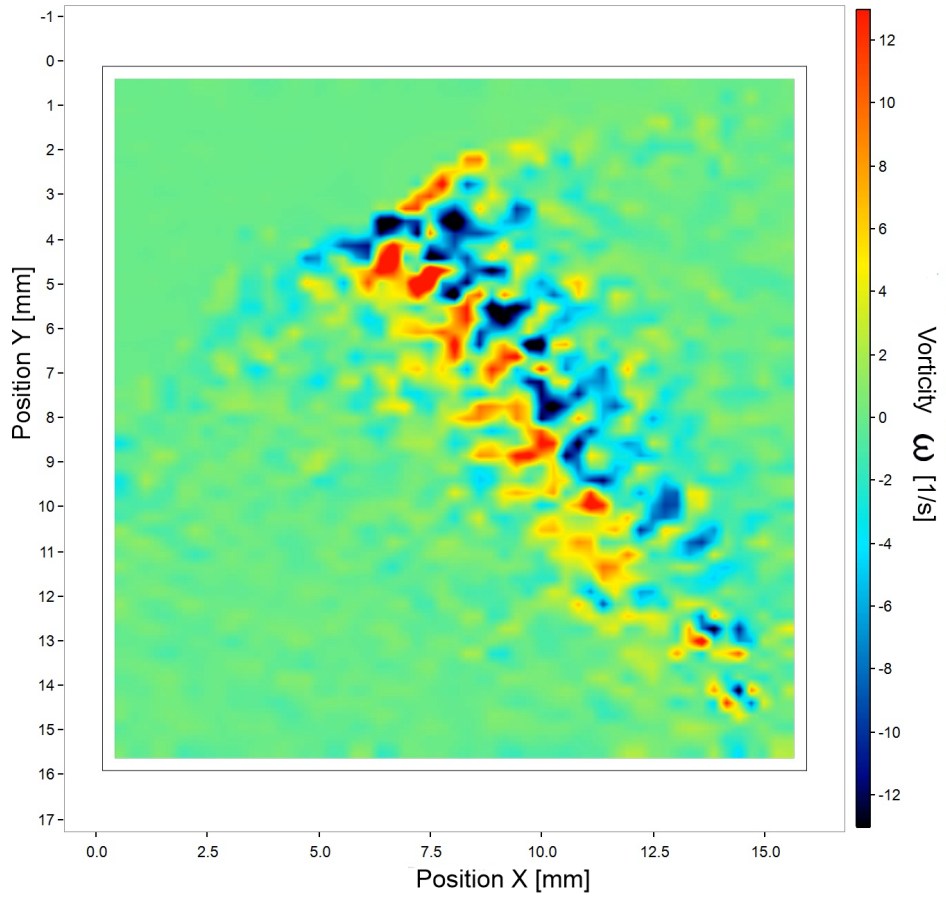

FIGURE 2. Map of vorticity in an electron-beam driven dust particle flow inside a quasi-2-dimensional plasma crystal.

There are multiple steps needed to take an input image and to then find the relevant contours in that image. First, we aim to separate color from brightness by converting blue-green-red (BGR) to hue-saturation-value (HSV) using the Python cv2.cvtColor() with the following syntax: `hsv_img = cv2.cvtColor(bgr_img, cv2.COLOR_BGR2HSV)` [30, 31]. This function converts RGB/BGR to HSV with H ranging from 0 to 180. This conversion allows us to selectively pick our red and blue hues and create a binary image mask $M(x, y)$ where our color range becomes white and everything else becomes black. Next, we must select our hues of red and blue which are of interest in

the image. Red and blue hues are isolated by applying lower L and upper U bounds as threshold values given by the following equation.

$$M(x,y) = \begin{cases} 1, & \text{if } \mathbf{L} \leq I_{\text{HSV}}(x,y) \leq \mathbf{U} \\ 0, & \text{otherwise} \end{cases}$$

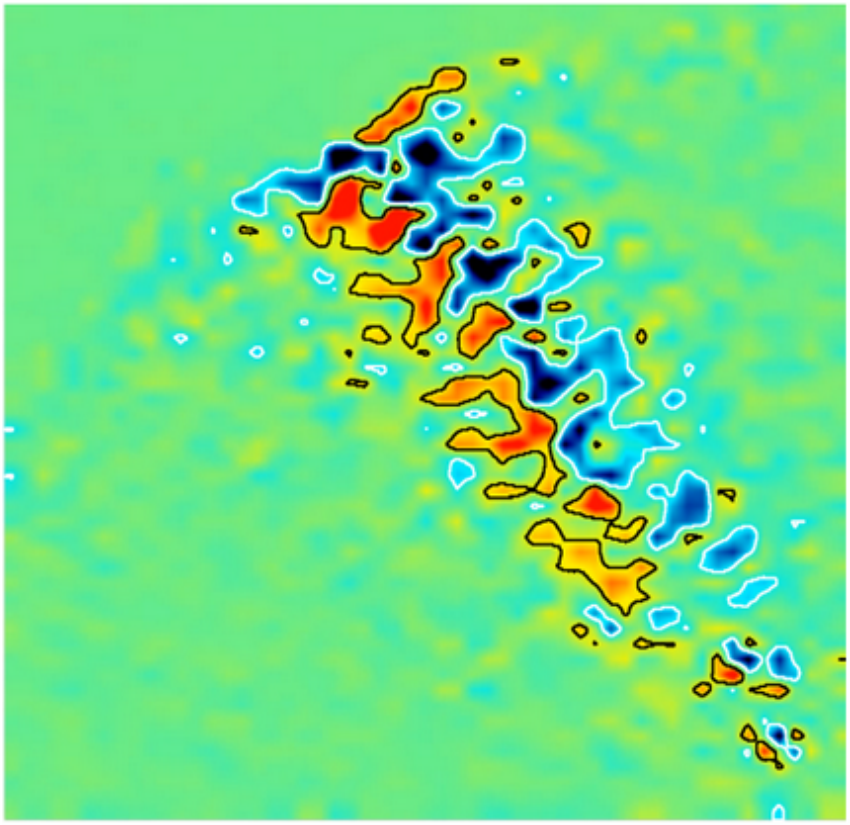

FIGURE 3. Post-processed image from Fig. 1, segmented into red and blue contours marked with black and white lines, respectively.

This threshold selection is done manually by trial and error to find our best values to use for our binary mask; our selected values are: Red $\mathbf{H} \in [0, 30] \cup [150, 180]$, and Blue $\mathbf{H} \in [90, 130]$. We then create a binary image dependent on whether pixels fall within our selected HSV color range using the function `cv2.inRange()`. This binary image becomes our image mask to use for finding contours with `cv2.findContours()` to trace red and blue contours.

The hue **H** represents the color type, encoded between 0 and 360° on the color wheel. In OpenCV, this range is scaled to 0–179 to fit within the 8-bit image format. The quantity I_{HSV} denotes the intensity components of hue **H**, saturation **S**, and value **V**. Both **S** and **V** range from 0 to 255, where **S**

corresponds to color purity (varying from gray to vivid color), and **V** represents the brightness level of the image. The complete color range is defined for hue values in [0,180]; selecting a hue value greater than 179 causes the value to wrap around to 0, which corresponds to red. In OpenCV, the red hue range used here is defined by [0,30] and [150,180], as the hue wraps around the zero point. The hue range used for blue is defined by [90,130]. The connection between hue and vorticity is illustrated in Figure 2, where color represents vorticity as indicated by the color bar on the right. In this representation, color is encoded in OpenCV hue values ranging from 0 to 180.

We apply principal component analysis (PCA) to the red and blue contours in the image to more effectively visualize the clustering of these shapes. PCA is a dimensionality reduction technique that constructs linear combinations of the original features, enabling visualization and analysis of high-dimensional data. In our case, the PCA vectors describe variations in color along the x and y directions. The first principal component (PC1) primarily captures the dominant features related to color and spatial distribution. This approach effectively generalizes patterns in the data while preserving essential information, making it especially useful when dealing with datasets that contain many features that are difficult to visualize or interpret directly.

4. **Results and Discussion**

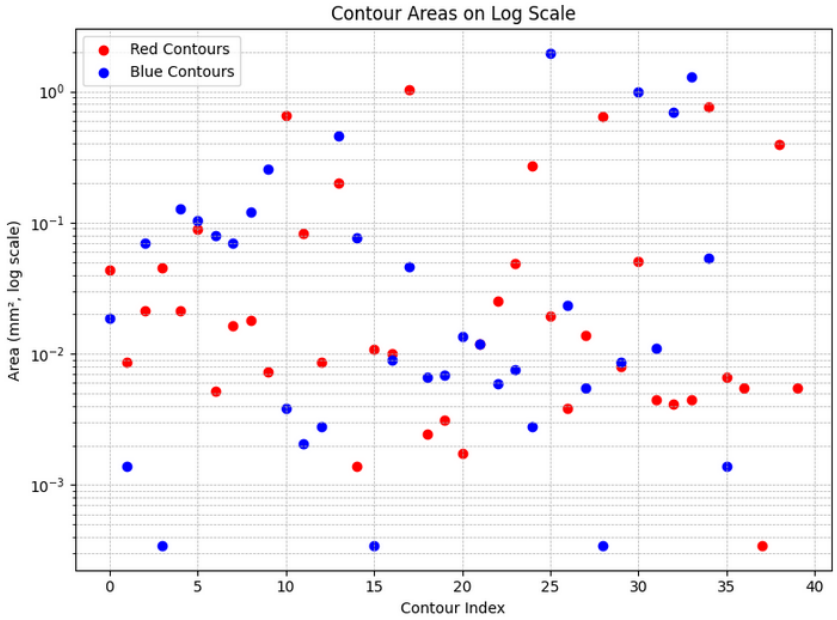

FIGURE 4. Scatter plot of red and blue contour areas.

Using the method described above, we identify 40 red contours (corresponding to regions of positive vorticity) and 36 blue contours (corresponding

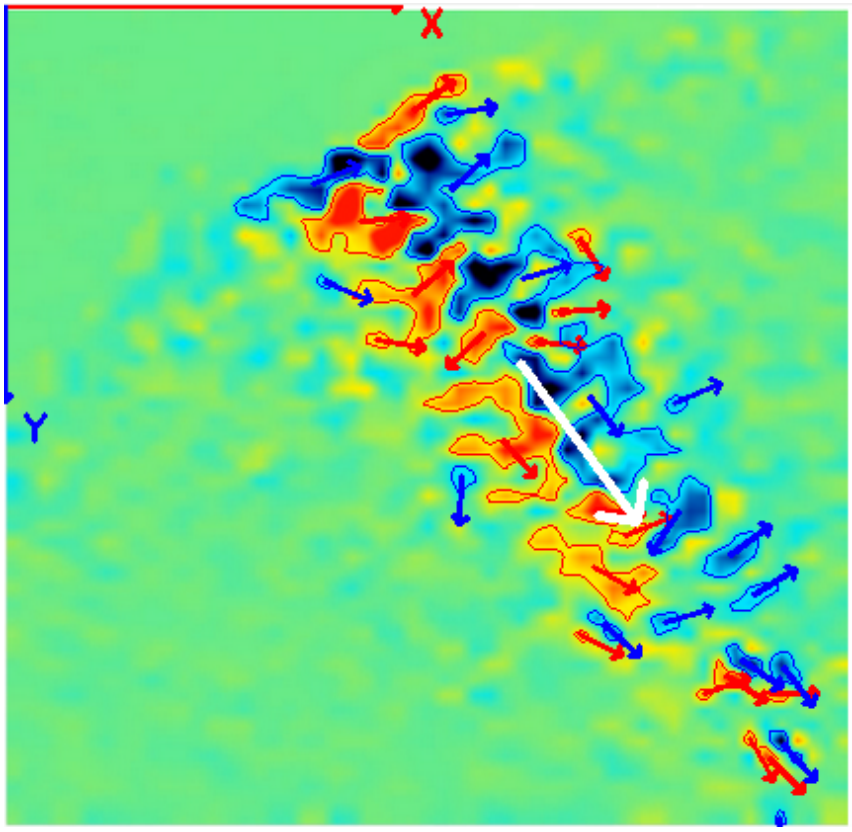

FIGURE 5. PCA vectors drawn over red and blue contours, with white global PCA vector drawn at an angle of 53.5° with OX axis which indicates the general flow direction.

to negative vorticity) with well-defined areas in Figure 3. A statistical analysis of the vortex contours and their associated areas is presented in Figure 4.

The contour index on the x-axis in Figure 4 represents the index number of each contour for both red and blue (number 0 for the first contour, 1 for the 2nd contour, etc). The smallest detected contours have areas of approximately 0.25×10^{-3} mm^2, while the largest reach up to 1 mm^2, spanning nearly three orders of magnitude in area.

In future work, a statistical analysis will be extended to encompass the full set of vorticities acquired at different time instances. The temporal evolution of vortex types (positive or negative) and their sizes will be crucial for characterizing the energy cascade and understanding how energy is transferred from large-scale vortices, driven by the action of the electron beam, to the smallest vortices, where it is ultimately dissipated as heat due to viscosity [26, 27, 32].

The PCA method provides dimensionality reduction, but in our case it allows for the visualization of some specific features in the turbulent dusty

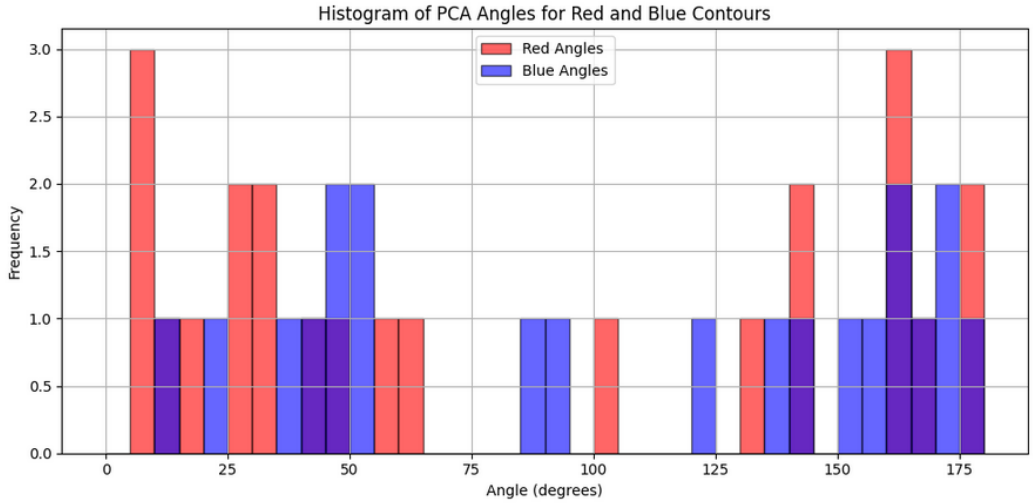

FIGURE 6. Histogram plot of red (with positive vorticity) and blue (with negative vorticity) vector PCA angles.

plasma flow. In Figure 5, the PCA vectors represent the elongation of the vortices, which is the direction of maximal variance. Here, PCA vectors represent the general preferred orientation of vortex structures. The PCA histogram shown in Figure 6 tells us about the distribution of orientations of the vorticity field throughout the image. The frequency on the y-axis indicates the number of times each contour occurs within the corresponding angle range on the x-axis.

OpenCV uses a pixel-based coordinate system for images. The angles are aligned to the x-axis as a reference where the top left corner of the image is (0,0), moving vertically downward is the positive y-direction (straight down is 90 degrees), and horizontally to the right is the positive x-direction (0 degrees), but angles increase clockwise. In OpenCV's reference: 0°= right, 90° = down, 180° = left, 270° = up.

Now, we add OpenCV's context to our histogram, in which angles past 180° are normalized to $[0°, 180°)$ to represent principal axes as found by PCA. In our histogram, we have removed the column representing angles $< 5°$ to avoid overlap with 180°. We notice in our histogram a relatively large number of values between 125° and 175° that are drawn at those angles in the image; these values are accounted for by the reverse angle by adding 180°. The global PCA vector (marked in white) is calculated to be at 53.5°. This vector represents the dominant direction of the vortex field overall, evidently induced by the e-beam; it is not represented in the histogram as it corresponds to the average of all vectors across the entire image. The broad distribution and apparent randomness of the PCA vectors provide additional evidence for the turbulent character of the dusty plasma flow.

5. Conclusion

This study demonstrates the effectiveness of computer vision-based analysis in identifying and characterizing vortex regions within turbulent, strongly coupled dusty plasma flows. High-energy pulsed electron beams with energy of about 13 keV induce complex Coulomb interactions between particles and the beam, driving turbulence in these flows. Our analyses utilize two-dimensional vorticity maps obtained by particle image velocimetry (PIV) that reveal a multitude of positive and negative vorticity regions, visualized in red and blue, respectively. By applying Python functions from the OpenCV library for object segmentation, we accurately delineated vortex contours and quantified their areas. Furthermore, principal component analysis (PCA) was employed to compute vorticity gradients within these regions, with PCA vectors overlaid on contours to illustrate vorticity orientation. A histogram of PCA angles across the image highlights the predominant vorticity orientations, providing insights into the statistical distribution of turbulent vortices. This study is an important step towards analyzing vorticity diffusion and understanding energy transfer scales in turbulent dusty plasmas. Future research will focus on real-time vortex tracking and the development of generative models to produce synthetic datasets, enhancing our ability to predict and model complex plasma dynamics.

Acknowledgments

This work was supported by the PN 23 21 01 05 contract sponsored by the Romanian Ministry of Research, Innovation and Digitalization, the IOSIN funds for research infrastructures of national interest, and project ELI-RO-19 "HighProton-PLas" funded by IFA.

REFERENCES

[1] *P.K. Shukla and B. Eliasson*, Colloquium: Fundamentals of dust-plasma interactions, Rev. Mod. Phys. **81**(2009), 25.

[2] *J.H. Chu, Lin I*, Direct observation of Coulomb crystals and liquids in strongly coupled rf dusty plasmas, Phys. rev. Lett **72**(1994), 4009.

[3] *G.E Morfill. B.M. Annaratone1, P. Bryant, A.V. Ivlev, H.M. Thomas, M. Zuzic, V.E. Fortov*, A review of liquid and crystalline plasmas—new physical states of matter? Plasma Phys. Control. Fusion **44**(2002), B263.

[4] *M. H. Thoma, M. Kretschmer, H. Rothermel, H. M. Thomas, G. E. Morfill*, The plasma crystal. Am. J. Phys. **73**(2005), No. 5, 420–424.

[5] *M. G. Hariprasad, P. Bandyopadhyay, G. Arora, A. Sen*, Experimental observation of a dusty plasma crystal in the cathode sheath of a DC glow discharge plasma. Phys. Plasmas **25**(2018), No. 12, 123704.

[6] *S. Jaiswal, C. Belt, A. Kananovich, E. M. Aguirre*, Structural transformation of dusty plasma crystal in dc discharge plasma by changing confinement ring bias, Phys. Rev. Res. **6** (2024), 013119.

[7] *R.L. Merlino, J.A. Goree*, Dusty Plasmas in the Laboratory, Industry, and Space, Physics Today **57**(2004), No. 7, 32–38.
[8] *J. Beckers, J. Berndt, D. Block, M. Bonitz, P.J. Bruggeman, et al.*, Physics and applications of dusty plasmas: The Perspectives 2023, Phys. Plasmas **30**(2023), 120601.
[9] *D. Ticos, E. Constantin, M.L. Mitu, A. Scurtu, C.M. Ticos*, A laboratory platform for studying rotational dust flows in a plasma crystal irradiated by a 10 keV electron beam. Sci. Rep. **13**(2023), 940.
[10] *A Piel, A Homann and A Melze,*Laser-excited waves in a plasma crystal, Plasma Phys. Control. Fusion **41**(1999) A453–A461.
[11] *L. Couedel, V. Nosenko, M Rubin-Zuzic, S. Zhdanov, Y Elskens, et al.* Full melting of a two-dimensional complex plasma crystal triggered by localized pulsed laser heating. Phys. Rev. E **97**(2018), No. 4, 043206.
[12] *A. Gavrikov , I. Shakhova, A. Ivanov, O. Petrov, N. VoronaV. Fortov*, Experimental study of laminar flow in dusty plasma liquid, Phys. Lett. A **336**(2005), No. 4–5, 378-383.
[13] *G. Uchida, S. Iizuka, N. Sato*, Liquid-crystal phase transition by electron shower in a direct current complex plasma, Phys. Plasmas **16**(2009), 083707.
[14] *E.V. Vasilieva, O.F. Petrov, M.M. Vasiliev*, Laser-induced melting of two-dimensional dusty plasma system in RF discharge., Sci. Rep. **11**(2021), 523.
[15] *Sergey I. Kopnin, Tatiana I. Morozova, Sergey I. Popel*, Electron Beam Action and High Charging of Dust Particles, IEEE Trans Plasma Sci **46**(2018), No. 4, 701-703.
[16] *A.F. Pal, A.V. Filippov, A.N. Starostin*, An experimental and theoretical study of the high-pressure dusty plasma created by a stationary e-beam, Plasma Phys. Control. Fusion **47**(2005), B603–B615. (2008).
[17] *A. V. Gavrikov, V. E. Fortov, O. F. Petrov, N. A. Vorona, and M. N. Vasiliev*, Experimental Studying of Dust Particles Charging by Electron Beam, AIP Conf. Proc. **1041**(2008), 337.
[18] D. Law, W.H. Steel, B.M. Annaratone, J.E. Allen, Probe-Induced Particle Circulation in a Plasma Crystal, Phys. Rev. Lett. **80**(1998), 4189.
[19] *C.M. Ticos, D. Ticos, J.D. Williams*, Kinetic effects in a plasma crystal induced by an external electron beam, Phys. Plasmas **26**(2019), 043702.
[20] *C.M. Ticos, D. Ticos, J.D. Williams*, Pushing microscopic matter in plasma with an electron beam Plasma Phys. Contr. Fusion **62**(2019), No. 2, 025003.
[21] *D. Ticos, A. Scurtu, J.D. Williams, L. Scott, E. Thomas Jr., D. Sanford, C.M. Ticos*, Rotation of a strongly coupled dust cluster in plasma by the torque of an electron beam, Phys. Rev. E **103** (2021), 023210.
[22] *E. Nebbat; R. Annou*, Vortices in non-ideal dusty plasmas, AIP Conf. Proc. **1397** (2011), 351–352.
[23] *Y. Bailung, B. Chutia, T. Deka, A. Boruah, S.K. Sharma, S.Kumar, J.Chutia, Y. Nakamura, H. Bailung*, Vortex formation in a strongly coupled dusty plasma flow past an obstacle, Phys. Plasmas **27** (2020), No. 12, 123702.
[24] *E. Nebbat, R. Annou, M.A. Bailiche*, On Vortices in Viscous Dusty Plasma With a Variable Dust Charge, Contrib. Plasma Phys. **65** (2025), e202400062.
[25] *M. Choudhary*, A review on the vortex and coherent structures in dusty plasma medium, J. Plasma Phys **91** (2025), No. 1, E7.
[26] *S. Sharma, R. Wani, P. Srivastav, M. Sharma, S. Bose, Y. Saxena, S. Tiwari*, Observation of Kolmogorov turbulence due to multiscale vortices in dusty plasma experiments, Phys. Plasmas **31** (2024), no. 12, 123704.

[27] *R.P.J. Kunnen, H.J.H. Clercx, B.J. Geurts*, Vortex statistics in turbulent rotating convection, Phys. Rev. E **82**(2010), 036306.
[28] *J.D. Williams*, Application of particle image velocimetry to dusty plasma systems, J. Plasma Phys **82**(2016), No. 3, 615820302.
[29] *R.C. Gonzalez, R.E. Woods*, Digital Image Processing, Pearson (2018).
[30] OpenCV Documentation: https://docs.opencv.org/
[31] *G. Bradski, A. Kaehler*, Learning OpenCV, O'Reilly Media (2008).
[32] *A.P. Almoguera, D. Kivotides*, Vortex dynamics of turbulent energy cascades. Phys. Fluids **36** (2024), No. 12, 125156.